Covid-19: Predicting inhibition of SARS-CoV-2 in Caco-2 cells: viral cellular entry

Clifford W Fong

Covid-19: Predicting inhibition of SARS-CoV-2 in Caco-2 cells: viral cellular entry

Clifford W. Fong

Eigenenergy, Adelaide, South Australia, Australia.
Email: cwfong@internode.on.net

Keywords: COVID-2019 or SARS-CoV-2; SARS-CoV; MERS; inhibition Caco-2 cells, ACE2 receptor binding, spike serine proteases, S-RBD, IC_{50}, host cell membrane fusion or endocytosis, TMPRSS2, linear free energy relationships, HOMO-LUMO; quantum mechanics;

Abbreviations: Structure activity relationships SAR, $\Delta G_{desolv,CDS}$ free energy of water desolvation, $\Delta G_{lipo,CDS}$ lipophilicity free energy, CDS cavity dispersion solvent structure of the first solvation shell, Dipole moment DM, Molecular Volume Vol, HOMO highest occupied molecular orbital, LUMO lowest unoccupied molecular orbital, HOMO-LUMO energy gap, linear free energy relationships LFER, Molecular docking binding energy BE, Receptor binding domain of S protein of SARS-CoV-2 S-RBD.

Abstract

A previously described quantum mechanical LFER model can be derived for a wide range of repurposed small molecule drugs which can inhibit SARS-CoV-2 in-vitro in human Caco-2 cells. There is evidence that this model applies to drugs acting as viral S-RBD inhibitors, TMPRSS2 host cell membrane fusion inhibitors and host cell ACE2 inhibitors. A similar LFER involving the lipophilicity, molecular volume and HOMO of the inhibitors can also be derived from available molecular docking binding energies for inhibitor-ACE2 and inhibitor-S-RBD interactions. The $HOMO_{inhibitor} \rightarrow LUMO_{receptor}$ is the dominant molecular interaction, not the $HOMO_{receptor} \rightarrow LUMO_{inhibitor}$. The inhibitor RS504393 has been shown to bind to the S-RBD of SARS-CoV-2 and ACE2 receptors. It is suggested that it may be possible to find other repurposed approved drugs that can inhibit viral S-RBD and host cell ACE2 receptors, and so provide therapeutic options to reduce infection by SARS-CoV-2 and other coronaviruses.

Introduction

The SARS-CoV-2 virus enters cells via the ACE2 receptor. [1-3] ACE2 is present in many cell types and tissues including the lungs, heart, blood vessels, kidneys, liver and gastrointestinal tract. It is present in epithelial cells. The crystallization of SARS-CoV-2 spike protein complexed to ACE2 has been structurally determined. [PDB 6M18] The enzyme ACE2 is an important protein that promotes tissue regeneration. It is known that ACE inhibitors and angiotensin receptor blockers (ARB) lead to increased formation of ACE2. Unfortunately, the coronavirus SARS-CoV-2 binds to this protein and uses it to enter cells, where it multiplies, similarly to SARS-Cov. Some patients with cardiac disease, hypertension or diabetes are treated with drugs that increase the amount of ACE2, and there is some controversy about whether patients using antihypertensives ACE inhibitors or ARB should maintain their regimen if they contact COVID-19. ARB are known to increase the expression of the ACE2 protein.

SARS-CoV-2 attaches to the host cell ACE2 receptor by way of the spike protein. Next, a part of the spike protein, called the fusion peptide, interacts directly with the host cell membrane and facilitates merging to form a fusion pore, or opening. The virus then transfers its genome into the host cell through this pore. These genomic instructions essentially commandeer the host's machinery to produce more viruses. Calcium ions interacting with the fusion peptide can change the peptide's structure, and how it interacts with membranes in ways that promote infection in MERS and SARS. SARS-CoV, MERS-CoV, and SARS-CoV-2 entry (receptor binding and membrane fusion) is governed by the viral spike (S) protein. The transmembrane serine 2 protease (TMPRSS2) on the cell surface is involved in S protein priming in lung cells. In other cells, such as kidney cells, the enzyme cathepsin L is required for the virus to infect them. TMPRSS2 and lysosomal cathepsins both have cumulative effects with furin on activating SARS-CoV-2 entry. The fusion peptide is well conserved across the CoV family, making it a good target for coronavirus antivirals. The biological sequences of the fusion peptides of SARS-CoV and SARS-CoV-2, are a 93% match. The virus can also enter the host cell by endocytosis after attaching itself to the ACE2 receptor and then engulfed by the cell membrane into the cellular cytoplasm. [1,2] Figure 1 illustrates membrane fusion and endocytosis mechanisms of viral cell entry.

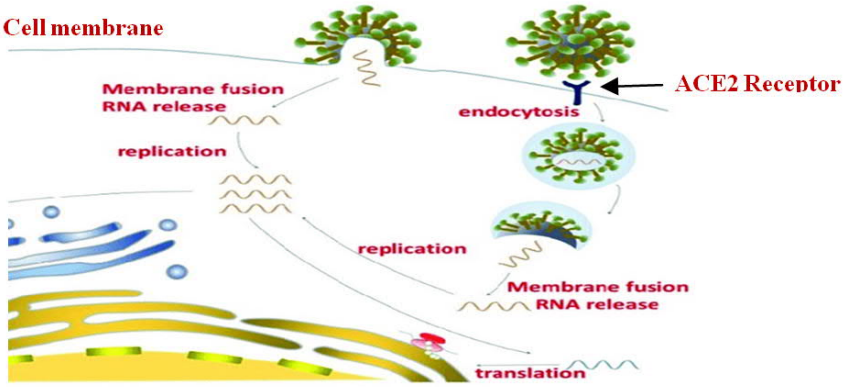

Figure 1. Membrane fusion and endocytosis mechanisms of viral cell entry

TMPRSS2 inhibitors approved for clinical use may block entry to the receptor and can constitute a treatment option against infection. Camostat mesylate, Nafamostat mesylate and Arbidol are known inhibitors of the TMPRSS2 membrane fusion related protease. The lysosomal cathepsin inhibitor E64d, as well as Camostat and Nafamostat also inhibit SARS-CoV-2 entry. [2-5,9] The drugs A1AT, BHH, and AEBS have also been found to inhibit TMPRSS2. [6]

ACE2 is an obvious molecular target to inhibit cell entry of SARS-CoV-2. ACE2 inhibitors are standard treatment for hypertension and chronic heart failure, but Chloroquine phosphate inhibits terminal phosphorylation of ACE2, and hydroxychloroquine elevates the pH in endosomes which are involved in virus cell entry. The triple combination of Cepharanthine/selamectin/mefloquine hydrochloride has been identified as a treatment for SARS-CoV-2. [3] Choudhary et al [7] have used a high throughput virtual screening approach to investigate FDA approved drugs against both the receptor binding domain of the virus spike protein (S-RBD) and the ACE2 host cell receptor. They found that GR 127935 hydrochloride

hydrate, GNF-5, RS504393, TNP, and eptifibatide acetate bound to the virus binding motifs of ACE2 receptor, and KT203, BMS195614, KT185, RS504393, and GSK1838705A bound to the receptor binding site on the viral S-protein.

Ellinger et al [8] investigated a collection of 5632 compounds including 3488 compounds which have undergone clinical investigations (marketed drugs, phases 1 -3, and withdrawn) for their inhibition of viral induced cytotoxicity using the human epithelial colorectal adenocarcinoma cell line Caco-2 and a SARS-CoV-2 isolate obtained from an individual originally exposed to the virus in the Wuhan region of China. A total of 64 compounds with IC_{50} <20 μM were identified in the primary screen, including 19 compounds with IC_{50} < 1 μM. ACE2 is expressed in Caco-2, Calu-3 and Vero-6 cells on the apical membrane domains. Primary screening was performed at 10μM compound concentration, at a virus multiplicity of infection (MOI) of 0.01 and a virus incubation period of 48 h, to ensure multiple viral replication cycles. It is thought that the assay procedure is able to confirm the activity of clinically relevant compounds against both viral entry and replication mechanisms. Remdesivir was found to show the same inhibition of SARS-CoV-2 in Caco-2 and Vero-6 cells (IC_{50} 0.77 μM), and interestingly, higher potency IC_{50} 0.07 μM in SARS-CoV and MERS.

Lanevskij [10] analyzed by multistep non-linear multiple regression a literature database of 1366 Caco-2 permeability coefficients (P_e) for 768 diverse drugs and drug-like compounds from varying experimental conditions (pH from 4.0 to 8.0) to develop a permeability model comprised of a minimal set of physicochemical descriptors: octanol-water log D, pKa, hydrogen bonding potential, and molecular size.

Kim [11] found that the permeability coefficient for a series of model peptides in Caco-2 cells was dependent on octanol-water lipophilicity and hydrogen bonding potential. Milanetti [12] found that an analysis of the dynamic distribution of water molecules around twenty-three neutral drugs at pH 7.4 by molecular dynamics simulations, correlated well with the permeability measured using the human colon adenocarcinoma (Caco-2) cell line assay.

Results

We have previously shown that the general equation 1 can successfully describe transport processes of drugs across the cell membrane. [13-17]

Eq 1

$$\text{Drug Transport} = \Delta G_{desolv,CDS} + \Delta G_{lipo,CDS} + \text{Dipole Moment} + \text{Molecular Volume}$$

The four independent molecular specifiers in eq 1 can be useful in screening how drugs might be transported across the host cellular membrane or block the virus-host membrane interaction that is critical for progressing COVID-2019 infection.

Eq 2

$$\text{Inhibition COVID-19} = \Delta G_{desolv,CDS} + \Delta G_{lipo,CDS} + \text{Dipole Moment} + \text{Molecular Volume} + \text{HOMO-LUMO}$$

Eq 2 can be applicable to the inhibition of the various proteases involved in the SARS-CoV-2, SARS-CoV and MERS-CoV replication process. We have previously shown [18-21] that the molecular specifiers used in eq 1 and eq 2 can be useful screening tools to evaluate the potential efficacy of therapeutic drugs that may be active against the SARS-CoV-2 virus.

Analysis of Ellinger's IC_{50} data for SARS-CoV-2 in Caco-2 cells [8] for 56 drugs (see Table 1) is shown below in eq 3(a)

Eq 3(a)

$$\mathbf{IC_{50} = 0.76\Delta G_{desolv,CDS} + 0.82\Delta G_{lipo,CDS} + 1.71 Mol\ Vol - 0.09(HOMO\text{-}LUMO) + 4.34}$$

Where R^2 = 0.174, SEE = 5.55, SE($\Delta G_{desolvCDS}$) = 0.30, SE($\Delta G_{lipoCDS}$) = 0.34, SE(Mol Vol) = 0.54, SE(HOMO-LUMO) = 0.73, F=2.69, Significance= 0.041

where $\Delta G_{desolv,CDS}$ is the free energy of water desolvation, $\Delta G_{lipo,CDS}$ is the lipophilicity free energy, the molecular volume in water, and HOMO-LUMO is the energy gap in water. No correlation was found with the dipole moment. The molecular volumes have been scaled by 35 times to allow a direct comparison of the relative magnitudes of the four molecular specifiers.

It is clear that eq 3(a) shows negligible dependency on the HOMO-LUMO gap, which can be eliminated to give eq 3(b) which is more significant by virtue of the elimination of the HOMO-LUMO variable:

Eq 3(b)

$$\mathbf{IC_{50} = 0.76\Delta G_{desolv,CDS} + 0.83\Delta G_{lipo,CDS} + 1.71 Mol\ Vol + 4.34}$$

Where R^2 = 0.174, SEE = 5.55, SE($\Delta G_{desolvCDS}$) = 0.30, SE($\Delta G_{lipoCDS}$) = 0.34, SE(Mol Vol) = 0.54, F=3.64, Significance= 0.018

It is noted that the p-values of the coefficients of the $\Delta G_{desolvCDS,}$ $\Delta G_{lipoCDS}$ and Molecular Volume molecular specifiers in eq 3(b) are significant at 0.015, 0.018 and 0.003 levels. The low regression coefficient is partly due to the low sensitivity of the coefficients to IC_{50}, since the regression coefficient is dependent on the slope of the regression line.

Eq 3(b) and 3(a) also includes 9 positively charged drugs and their neutral counterparts, since these drugs can be charged at neutral pH conditions in vitro.

Using Choudhary's molecular docking binding energy [7] of 10 drugs (Table 2) to the SARS-CoV-2 ACE2 receptor gives eq 4(a); no significant dependencies with $\Delta G_{desolvCDS,}$ or dipole moment were found.

Eq 4(a)

$$\mathbf{Binding\ Energy\ (ACE2) = -1.34\Delta G_{lipo,CDS} - 0.80 Mol\ Vol + 1.93 HOMO\text{-}LUMO - 27.05}$$

Where R^2 = 0.51, SEE = 1.88, SE($\Delta G_{lipoCDS}$) = 0.64, SE(Mol Vol) = 0.68, SE(HOMO-LUMO)= 1.53 , F=2.15, Significance= 0.195

Eq 4(b) substituting HOMO for the HOMO-LUMO gap gives an improved correlation:

$$\mathbf{Binding\ Energy\ (ACE2) = -1.14\Delta G_{lipo,CDS} - 0.58 Mol\ Vol - 8.35 HOMO - 64.72}$$

Where R^2 = 0.73, SEE = 1.42, SE($\Delta G_{lipoCDS}$) = 0.33, SE(Mol Vol) = 0.30, SE(HOMO)= 3.08 , F=5.29, Significance= 0.040

The BE dependency on molecular volume is poor, and not significant. It is noted that a much poorer correlation is found with LUMO (compared to HOMO) which is reflected in the weaker relationship with the HOMO-LUMO gap in eq 4(a)

Using Choudhary's molecular docking binding energy [7] of 6 drugs (Table 2) to the SARS-CoV-2 S-RBD gives eq 5; no significant dependencies with $\Delta G_{desolvCDS}$ or dipole moment were found. The correlations with HOMO-LUMO or LUMO were much weaker.

Eq 5(a)

Binding Energy (S-RBD) = 2.585HOMO + 6.83

Where R^2 = 0.958, SEE = 0.22, SE(HOMO)= 0.27 , F=90.98, Significance= 0.00067

Eq 5(b) including $\Delta G_{desolvCDS}$ and molecular volume gives:

Binding Energy (S-RBD) = 0.11$\Delta G_{lipo,CDS}$ + 0.15Mol Vol + 2.845HOMO + 8.66

Where R^2 = 0.981, SEE = 0.21, SE($\Delta G_{lipoCDS}$) = 0.075, SE(Mol Vol) = 0.01, SE(HOMO)= 0.32 , F=33.68, Significance= 0.029

Comparison of eqs 4(b) for the ACE2 binding energy and 5(b) for the S-RBD binding energy shows a reversal of sign for the three independent variables with far greater opposite dependence on the HOMO in eq 5(b) compared to eq 4(b). These eqs indicate a substantial difference between the inhibitor binding interactions of the viral S-RBD and the ACE2. We have previously shown that the binding energy of a series of protease inhibitors is well correlated with the HOMO-LUMO energy gap and the molecular volume of the inhibitors. [21]

By combining the 16 data for the ACE2 and S-RBD binding gives eq 6:

Eq 6:

Binding Energy (ACE2+S-RBD) = -0.70$\Delta G_{lipo,CDS}$ - 0.15Mol Vol - 1.75HOMO + 8.66

Where R^2 = 0.375, SEE = 1.675, SE($\Delta G_{lipoCDS}$) = 0.31, SE(Mol Vol) = 0.01, SE(HOMO)= 1.86 , F=2.21, Significance= 0.118

It can be seen that eq 6 is a much poorer correlation than either eq 4(b) or 5(b), reinforcing that two very distinct interactions are occurring in the binding of drugs to ACE2 and S-RBD.

Discussion

Eq 3(a) derived from the IC_{50} data for SARS-CoV-2 in Caco-2 cells for 56 drugs indicates that a high precision LFER can be constructed for a very wide range of repurposed inhibitor drugs. Ellinger's experimental conditions involved initial additions of the drugs to the Caco-2 cells followed by infection by SARS-CoV-2 for 48 hours. [8] Under these conditions it is likely that interactions can occur amongst (a) inhibitors and virus, (b) inhibitors and ACE2 and or TMPRSS2 receptors of the Caco-2 cells, (c) virus infection of the Caco-2 cell through the ACE2 receptor: cell membrane fusion and/or endocytosis of the virus into the Caco-2 cell, and (d) transport of the inhibitors into the infected Caco-2 cell to interfere with viral replication processes.

Eq 3(a) and (b) with dependencies on the molecular specifiers $\Delta G_{desolvCDS,}$ $\Delta G_{lipoCDS}$ and molecular volume are consistent with previous studies of drug transport across Caco-2 membranes. [10-12]

Eqs 4(b) and 5(b) show how the docking binding energy for the inhibitor-ACE2 complex compares to the inhibitor-S-RBD complex. The same form of the LFER applies to both systems, but the reversal of signs clearly shows a different binding interaction, with the larger dependence on the HOMO for the ACE2 binding. The dependence on the HOMO rather than LUMO or HOMO-LUMO gap in eq 4(b) and 5(b) suggests that $HOMO_{inhibitor} \rightarrow LUMO_{receptor}$ is the dominant molecular interaction, not the $HOMO_{receptor} \rightarrow LUMO_{inhibitor}$. It is noted that Choudhary found the inhibitor RS504393 was more weakly bound to S-RBD of SARS-CoV-2 (BE -7.57 kcal/mol) than to ACE2 (BE -8.32 kcal/mol).

We have previously shown that the in situ interaction between a wide range of repurposed inhibitors and the protease involved in viral replication inside infected host cells can be described by the general eq 2 for members of the coronaviridae family, with the HOMO-LUMO energy gap being particularly important for the SARS-Cov-2. [18-21] So it seems anomalous that eq 3(a) shows such a weak statistical dependence on the HOMO-LUMO gap. However, since inhibitor-ACE2 and inhibitor-S-RBD interactions can both occur under the experimental conditions, it seems that eqs 4(b) and 5(b) may both be applicable under the conditions that apply to the derivation of eq 3(a), ie both inhibitor-ACE2 and inhibitor-S-RBD interaction can occur at the same time. Eq 6 has been constructed to simulate this event, showing how dependence on the HOMO is neutralized because of the opposing dependence on the HOMO in eq 4(b) and 5(b).

Wang [9] has discussed the potential for broad-spectrum corona fusion inhibitors, including peptides, proteases, antibodies and small molecule inhibitors, such as Camostat and Nafamostat. It is noted that Nafamostat mesylate and Camostat mesylate which are included in the 56 drugs used to derive eq 3(a) have been previously shown to be TMPRSS2 cell membrane fusion inhibitors in Calu-3 and Vero cells, and in vivo with BALB/c mice for Camostat. [9] Other TMPRSS2 inhibitors have been identified. [6] The observations as described in eq 3(a), 4(b) and 5(b) suggest that Ellinger's experimental data involves both inhibitor-ACE2 and inhibitor-TMPRSS2 concurrent interactive processes. Eq 3(a) is consistent with drugs interacting with either the virus S-RBD, or host cell ACE2 or TMPRSS2 receptors, or transport processes of drugs across the host cell membranes either by passive or active (endocytosis) mechanisms.

Conclusions

It has been shown that a previously described quantum mechanical LFER model can be derived for a wide range of repurposed small molecule drugs which can inhibit SARS-CoV-2 in-vitro in human Caco-2 cells. There is evidence that this model applies to drugs acting as viral S-RBD inhibitors, TMPRSS2 host cell membrane fusion inhibitors and host cell ACE2 inhibitors. A similar LFER involving the lipophilicity, molecular volume and HOMO of the inhibitors can also be derived from available molecular docking binding energies for inhibitor-ACE2 and inhibitor-S-RBD interactions. The $HOMO_{inhibitor} \rightarrow LUMO_{receptor}$ is the dominant molecular

interaction, not the $HOMO_{receptor} \rightarrow LUMO_{inhibitor}$. The inhibitor RS504393 has been shown to bind to the S-RBD of SARS-CoV-2 and ACE2 receptors. It is suggested that it may be possible to find other repurposed approved drugs that can inhibit viral S-RBD and host cell ACE2 receptors, and so provide therapeutic options to reduce infection by SARS-CoV-2 and other coronaviruses.

Experimental Methods

All calculations were carried out using the Gaussian 09 package. Energy optimizations were at the DFT/B3LYP/6-31G(d) (6d, 7f) level of theory for all atoms in water. Selected optimizations at the DFT/B3LYP/6-311+G(d,p) (6d, 7f) level of theory gave very similar results to those at the lower level. Optimized structures were checked to ensure energy minima were located, with no imaginary frequencies. Energy calculations were conducted at the DFT/B3LYP/6-31G(d,p) (6d, 7f) for neutral and cationic compounds with optimized geometries in water, using the IEFPCM/SMD solvent model. With the 6-31G* basis set, the SMD model achieves mean unsigned errors of 0.6 - 1.0 kcal/mol in the solvation free energies of tested neutrals and mean unsigned errors of 4 kcal/mol on average for ions. [22] The 6-31G** basis set has been used to calculate absolute free energies of solvation and compare these data with experimental results for more than 500 neutral and charged compounds. The calculated values were in good agreement with experimental results across a wide range of compounds. [23,24] Adding diffuse functions to the 6-31G* basis set (ie 6-31+G**) had no significant effect on the solvation energies with a difference of less than 1% observed in solvents, which is within the literature error range for the IEFPCM/SMD solvent model. HOMO and LUMO calculations included both delocalized and localized orbitals (NBO).

It is noted that high computational accuracy for each species in different environments is not the focus of this study, but comparative differences between various species is the aim of the study. Experimental errors in inhibitory studies are substantially higher than those in calculated molecular specifiers.

References

[1] T Tang, M Bidon, JA Jaimes, GRWhittaker, S Daniel, Coronavirus membrane fusion mechanism offers a potential target for antiviral development, Antiviral Research, 2020, 178, 104792
[2] J Shang, Y Wan, C Luo, G Ye, Q Geng, A Auerbach, F Li, Cell entry mechanisms of SARS-CoV-2, PNAS, 2020, 117, 11727–11734
[3] DL McKee, A Sternberg, U Stange, S Laufer, C Naujokat, Candidate drugs against SARS-CoV-2 and COVID-19, Pharmacol Res, 2020, 157, 104859
[4] M Wang, R Cao, L Zhang et al, Remdesivir and chloroquine effectively inhibit the recently emerged novel coronavirus (2019-nCoV) in vitro, Cell Research 2020, 30, 269–271, doi:10.1038/s41422-020-0282- 0
[5] M Hoffmann, H Kleine-Weber, S Schroeder, et al. SARS-CoV-2 Cell Entry Depends on ACE2 and TMPRSS2 and Is Blocked by a Clinically Proven Protease Inhibitor, Cell, 2020, 181, 271–280.e8.

[6] NP Azouz, AM Klinger, ME Rothenberg, Alpha 1 Antitrypsin is an Inhibitor of the SARS-CoV2–Priming Protease TMPRSS2, bioRxiv preprint, 2020, doi: https://doi.org/10.1101/2020.05.04.077826.
[7] S Choudhary, YS Malik, S Tomar, Identification of SARS-CoV-2 Cell Entry Inhibitors by Drug Repurposing Using *in silico* Structure-Based Virtual Screening Approach, Front. Immunol., 2020, https://doi.org/10.3389/fimmu.2020.01664
[8] B Ellinger, D Bojkova, A Zaliani et al, Identification of inhibitors of SARS-CoV-2 in-vitro cellular toxicity in human (Caco-2) cells using a large scale drug repurposing collection, Research Square, 2020, doi: 10.21203/rs.3.rs-23951/v1
[9] X Wang , S Xia, Q Wang, W Xu, W Li, L Lu, S Jiang, Broad-Spectrum Coronavirus Fusion Inhibitors to Combat COVID-19 and Other Emerging Coronavirus Diseases, Int. J. Mol. Sci. 2020, 21, 3843; doi:10.3390/ijms21113843
[10] K Lanevskij, R Didziapetris, Physicochemical QSAR Analysis of Passive Permeability Across Caco-2 Monolayers, J Pharm Sci 2019, 108, 78-86
[11] DS Kim, PS Burton, RT Borchardt, A correlation between the permeability of a series of peptides using an in vitro cell culture model Caco-2 and those using an in situ perfused rat ileum culture model of the intestinal mucosa, Pharm Res 1993, 10, 1710-15
[12] E Milanetti, D Raimondo, A Tramontano, Prediction of the permeability of neutral drugs inferred from their solvation properties, Bioinformatics, 2016, 32, 163–1169
[13] CW Fong, Permeability of the Blood–Brain Barrier: Molecular Mechanism of Transport of Drugs and Physiologically Important Compounds, J Membr Biol. 2015, 248,651-69.
[14] CW Fong, The extravascular penetration of tirapazamine into tumours: a predictive model of the transport and efficacy of hypoxia specific cytotoxic analogues and the potential use of cucurbiturils to facilitate delivery, Int J Comput Biol Drug Design. 2017, 10, 343-373
[15] CW Fong, Statins in therapy: Understanding their hydrophilicity, lipophilicity, binding to 3-hydroxy-3-methylglutaryl-CoA reductase, ability to cross the blood brain barrier and metabolic stability based on electrostatic molecular orbital studies. Eur J Med Chem. 2014, 85, 661-674
[16] CW Fong, Predicting PARP inhibitory activity – A novel quantum mechanical based model. HAL Archives. 2016, https://hal.archives-ouvertes.fr/hal-01367894v1.
[17] CW Fong, A novel predictive model for the anti-bacterial, anti-malarial and hERG cardiac QT prolongation properties of fluoroquinolones, HAL Archives. 2016, https://hal.archives-ouvertes.fr/hal-01363812v1
[18] CW Fong, Inhibition of COVID-2019 3C-like protease: structure activity relationship using quantum mechanics, hal archives 2020, hal-02529030v1
[19] CW Fong, Screening potential repurposed COVID-2019 3C-like protease inhibitors**,** hal archives 2020, hal-02663287v1
[20] CW Fong, Screening potential anti-virals for the main protease of the Coronaviridae family including SARS-CoV-2, SARS-CoV, MERS, hal archives 2020, hal-02897882v1
[21] CW Fong, COVID-19: predicting inhibition of the main protease and therapeutic intracellular accumulation and plasma and lung concentrations of repurposed inhibitors**,** hal archives 2020, hal-02917312v1

[22] AV Marenich, CJ Cramer, DJ Truhlar, Universal Solvation Model Based on Solute Electron Density and on a Continuum Model of the Solvent Defined by the Bulk Dielectric Constant and Atomic Surface Tensions, J Phys Chem B, 2009, 113, 6378 -96
[23] S Rayne, K Forest, Accuracy of computational solvation free energies for neutral and ionic compounds: Dependence on level of theory and solvent model, Nature Proceedings, 2010, http://dx.doi.org/10.1038/npre.2010.4864.1.
[24] RC Rizzo, T Aynechi, DA Case, ID Kuntz, Estimation of Absolute Free Energies of Hydration Using Continuum Methods: Accuracy of Partial Charge Models and Optimization of Nonpolar Contributions, J Chem Theory Comput. 2006, 2, 128-139

Table 1. Inhibition of SARS-CoV-2 in human Caco-2 cells [8] and calculated molecular specifiers of repurposed drugs

Inhibitors	**IC_{50}** µM	**$\Delta G_{desolvCDS}$** kcal/mol	**$\Delta G_{lipoCDS}$** kcal/mol	**Dipole Moment D**	**Molec Vol cm^3/mol**	**HOMO eV**	**LUMO eV**	**HOMO-LUMO eV**
AI-10-49	0.19	-8.83	-10.44	6.93	452	-5.87	-1.61	4.26
Almatrine	1.42	-6.42	-17.17	2.4	357	-5.69	-0.38	5.31
Almatrine Ion	1.42	-8.04	-17.17	11.11	402	-6.12	-0.66	5.45
Alvocidib	0.59	-5.45	-8.96	6.43	261	-5.76	-1.53	4.24
Amuvatinib	0.02	-8.21	-12.37	9.35	230	-5.60	-1.05	4.55
Avasimibe	3.93	-11.74	-10.74	9.66	387	-6.21	-0.53	5.68
Avotrombopag	5.71	-7.09	-16.42	8.9	439	-4.89	-1.57	3.32
Camostat	0.64	-9.3	-10.48	11.4	256	-5.78	-1.41	4.36
Camostat Ion	0.64	-10.69	-10.7	43.64	274	-6.69	-2.03	4.66
Carboxyanidotriazole	0.09	-7.03	-7.57	4.78	237	-5.95	-2.20	3.75
Cetylpyridinium Ion	0.62	-8.08	-11.3	33.17	247	-7.66	-2.05	5.60
Chlormidazole	1.89	-3.49	-7.85	5.13	169	-6.02	-0.40	5.62
Dapivirine	0.73	-8.21	-10.73	9.35	230	-5.60	-1.05	4.55
DCPIB	12.78	-9.32	-10.86	12.71	337	-6.70	-1.83	4.87
Drotaverine	6.07	-9.57	-9.6	2.9	287	-4.71	-1.00	3.70
Drotaverine Ion	6.07	-10.75	-9.61	12.2	311	-5.75	-1.85	3.90
Ethaverine	0.64	-9.31	-9.4	5.27	311	-5.95	-1.34	4.61
GSK2606414	0.25	-7.49	-12.22	4.64	324	-5.19	-0.72	4.47
Hematoporphyrin	1.85	-14.61	-14.69	4.75	402	-3.57	-1.96	1.62
IPAG	5.96	-3.56	-8.68	4.01	202	-5.48	-0.67	4.81
JTE-013	5.97	-7.12	-9.79	7.57	260	-5.76	-0.97	4.79
Ketoconazole	2.36	-7.84	-12.65	7.49	405	-2.29	-0.86	1.43
LGK-974	3.27	-3.92	-9.02	8.7	266	-6.20	-1.79	4.40
Lidoflazine	17.39	-6.22	-11.84	6.25	401	-5.90	-0.30	5.60
Lidoflazine Ion	17.39	-6.22	-12.01	6.25	401	-5.90	-0.30	5.60
LY2228820	0.87	-6.03	-11.44	12.83	325	-4.95	-1.02	3.92
Mefloquine	14.15	-6.4	-4.33	9.43	259	-6.05	-2.09	3.95

Mefloquine Ion	14.15	-8.88	-4.53	28.78	216	-6.85	-2.22	4.62
Methylene Blue Ion	2.03	-3.89	-7.06	4.12	191	-5.61	-3.24	2.37
Nafamostat	0.04	-6.33	-9.19	4.18	256	-5.87	-1.83	4.04
Nafmostat DiIon	0.04	-9.51	-0.38	19.85	227	-6.19	-2.13	4.06
Papaverine	1.1	-9.15	-5.52	4.08	229	-5.97	-1.33	4.64
Pevonedistat	0.63	-5.53	-12.73	12.82	323	-5.39	-0.39	5.00
Pexidartinib	5.43	-5.3	-8.72	11.11	278	-5.36	-1.14	4.22
Polydocanol	0.22	-14.1	-15.32	0.35	492	-6.93	1.42	8.35
Regorafenib	1.67	-10.16	-7.87	8.02	291	-6.19	-1.60	4.59
SB-612111	0.77	-5.49	-11.31	3.86	316	-5.79	-0.52	5.28
SB-612111 DiIon	0.77	-7.7	-11.36	7.56	300	-6.29	-0.62	5.68
Sorafenib	1.55	-10	-9.74	8.32	292	-5.77	-1.42	4.35
Thioguanosine	0.78	-1.15	-9.39	10	157	-5.74	-1.02	4.72
Tioguanine	1.71	0.2	-7.81	10.38	95	-5.55	-1.33	4.22
Tyrphostin	0.2	-7.97	-2.04	9.83	131	-6.01	-2.43	3.58
VLX600	0.24	-1.99	-9.6	6.42	257	-5.64	-1.86	3.78
ZK-93423	1.34	-8.69	-9.25	5.66	308	-5.80	-1.42	4.38
Emetine	0.52	-7.07	-8.41	3.17	321	-5.42	-0.04	5.38
Emetine DiIon	0.52	-13.01	-8.68	16.13	313	-5.83	-0.34	6.17
Cycloheximide	0.58	-8.11	-6.81	9.1	239	-6.65	-0.93	5.72
Remdesivir	0.76	-13.44	-10.79	12.76	381	-5.97	-1.19	4.78
GS441524	0.76	-5.39	-4.83	7.65	166	-5.96	-1.17	4.79
Adoprazine	18.59	-3.7	-9.1	2.08	322	-5.14	-0.93	4.20
Aldoprazine Ion	18.59	-6.09	-9.16	8.12	281	-5.43	-1.16	4.27
AMG-9180	14.97	-8.87	-8.56	6.6	271	-5.48	-1.68	3.80
Apixavan	5.91	-10.05	-10.55	11.21	336	-5.92	-1.55	4.37
CC-223	16.78	-5.15	-9.29	3.3	306	-5.44	-1.32	4.11
LDE225	10.67	-10.28	-10.68	1.43	331	-5.12	-1.13	3.99
Loratadine	15.13	-7.08	-9.8	3.68	299	-6.05	-0.86	5.19

Footnotes: IC_{50} values for charged species assumed to be the same as uncharged species.

Table 2. Cell entry inhibitor binding energies to ACE2 and TMPRRS2 receptors [7] and calculated molecular specifiers of repurposed drugs

Inhibitor ACE2	**Binding Energy kcal/mol**	**$\Delta G_{desolvCDS}$** kcal/mol	**$\Delta G_{lipoCDS}$** kcal/mol	**Dipole Moment D**	**Molec Vol cm^3/mol**	**HOMO eV**	**LUMO eV**	**HOMO-LUMO eV**
GR127935 alt config	-11.23	-6.68	-11.5	4.42	360	-5.36	-1.68	3.68
GR127935 Ion alt config	-11.23	-10.67	-11.69	38.94	334	-5.54	-1.70	3.85
GR127935	-11.23	-6.17	-12.22	2.75	322	-5.21	-1.61	3.60
GR127935 Ion	-11.23	-10.46	-11.36	24.61	344	-5.41	-1.64	3.77
GNF-5	-7.57	-8.55	-10.38	11.94	243	-5.65	-1.54	4.12
RS504393	-8.32	-5.94	-9.98	10.36	315	-5.72	-1.16	4.56

TNP	-7.42	-6.99	-13.51	11.81	266	-5.18	-3.05	2.13
TNP alt config	-7.42	-7.96	-14.2	6.36	228	-5.30	-3.02	2.28
Eptifibatide Ion	-6.05	-14	-16.12	46.92	531	-5.65	-1.06	4.59
Eptifibatide	-6.05	-12.8	-15.72	6.76	637	-5.64	-1.04	4.61
Inhibitor TMPRSS2	**Binding Energy kcal/mol**	**$\Delta G_{desolvCDS}$** kcal/mol	**$\Delta G_{lipoCDS}$** kcal/mol	**Dipole Moment D**	**Molec Vol cm^3/mol**	**HOMO eV**	**LUMO eV**	**HOMO-LUMO eV**
KT203	-8.73	-9.73	-13.02	3.88	322	-5.91	-1.53	4.38
BMS195614	-8.25	-9.03	-12.01	15.5	322	-5.80	-1.77	4.03
KT185	-8.16	-8.53	-14.47	12.6	454	-5.87	-1.25	4.62
RS504393	-7.67	-5.94	-9.98	10.36	315	-5.72	-1.16	4.56
GSK1838705A	-6.46	-8	-14.6	12	402	-5.12	-1.07	4.04
GSK1838705A Ion	-6.46	-12.18	-14.85	39.12	329	-5.15	-1.09	4.06

Footnotes: Alternate configurations were tested for significant changes to molecular specifier properties. Binding energies of charged inhibitors were assumed to be the same as uncharged species.